ARTICLES

Functional Roles of the Heme Architecture and Its Environment in Tetraheme Cytochrome *c*

HIDEO AKUTSU* AND YUKI TAKAYAMA

Institute for Protein Research, Osaka University, 3-2 Yamadaoka, Suita 565-0871, Japan

Received January 30, 2006

ABSTRACT

Cytochromes are involved in a wide variety of redox reactions in living systems. Some of them contain multiple hemes such as *Desulfovibrio* cytochrome c_3 and *Shewanella* small tetraheme cytochrome *c*. The significance of *c*-type tetraheme architectures was discussed. A cyclic heme architecture and its environment regulate the extremely low redox potentials of cytochrome c_3 in addition to bis-imidazole coordination and heme exposure. Each heme in cytochrome c_3 plays a different role in the electron transport to/from [NiFe] hydrogenase and the specific CO-binding. In contrast, the chain-like heme architecture in *Shewanella* small tetraheme cytochrome *c* and soluble fumarate reductase provides a pathway for directional electron transfer. Thus, the tetraheme architectures do not comprise simple heme assemblies but sophisticated devices.

Introduction

Cytochromes are ubiquitous proteins that are involved in a wide variety of redox reactions in most living cells. Some cytochromes have multiple hemes, generally protoporphyrins coordinated to iron. Multiheme cytochromes are mainly found in bacteria, the ancestors of which can be

Hideo Akutsu is a professor at the Institute for Protein Research, Osaka University (Japan), and has served as the director of the Institute for 2004−2006. He is working on biological energy conversion systems and membrane systems, using solution and solid-state NMR as well as electrochemistry.

Yuki Takayama is a postdoctoral fellow at the Institute for Protein Research, Osaka University. His interests include electron transport mechanisms, molecular biology, and NMR.

traced back more than 500 million years to the anaerobic world. When oxygen began to accumulate in the biosphere, many anaerobes died. The multiheme architectures of some cytochromes may be responsible for the survival of some anaerobic bacteria, even as the environmental oxidation state changed. This Account describes the multiheme architectures in *c*-type cytochromes that have hemes covalently linked to polypeptides.

The most extensively investigated tetraheme cytochrome is cytochrome c_3 (cyt c_3) from sulfate-reducing bacteria, which are absolute anaerobes.[1] Cyt c_3 has been classified as a class III *c*-type cytochrome. The three-dimensional structures of various *c*-type multiheme cytochromes in the cyts c_3 superfamily have been determined as summarized in a report.[2] Their heme architectures are almost identical. Four hemes are located in a cyclic manner (Figure 1A). One of the most important properties of cyt c_3 is its extremely low reduction potential (~ -300 mV) in comparison with those of monoheme cyts *c* (about $+260$ mV for mitochondrial cyt *c*). Because cyt c_3 possesses four hemes, there are five oxidation states (S_0–S_4) and 16 molecular redox species, as shown in Figure 2. The reduction potentials characterizing the reduction of a molecule are termed macroscopic.[3] They are summarized in Table 1 for various cyts c_3. In contrast, microscopic reduction potentials characterize the reductions of individual hemes in each macroscopic oxidation state, as shown in Figure 2.[3] They have been estimated by the combined use of nuclear magnetic resonance (NMR) spectroscopy and electrochemistry for *Desulfovibrio vulgaris* Miyazaki F (*Dv*MF) cyt c_3 (Table 2).[3] Those for *D. vulgaris* Hildenborough (*Dv*H) have also been investigated by Xavier and his colleagues.[4]

In addition to cyts c_3, small tetraheme cytochrome (STC) and soluble fumarate reductase (SFR) from *Shewanella* species, cytochrome c_{554} from *Nitrosomonas europaea*, and cytochrome *c* attached to the photosyn-

* To whom correspondence should be addressed. Phone: +81-6-6879-8597. Fax: +81-6-6879-8599. E-mail: akutsu@protein.osaka-u.ac.jp.
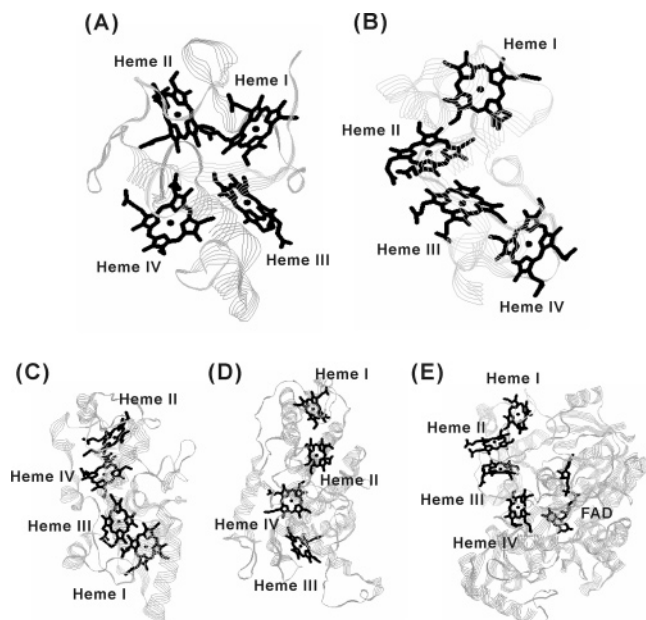
FIGURE 1. Tetraheme architectures in (A) cytochrome c_3 from *Desulfovibrio vulgaris* Miyazaki F, (B) small tetraheme cytochrome *c* from *Shewanella oneidensis*, (C) cytochrome c_{554} from *Nitrosomonas europaea*, (D) photosynthetic reaction center cytochrome subunit from *Rhodopseudomonas viridis*, and (E) soluble fumarate reductase from *Shewanella oneidensis* (with flavin adenine dinucleotide). The PDB entries are 1J0O, 1M1P, 1FT5, 1PRC, and 1D4C, respectively.

thetic reaction center (RCC) in photosynthetic bacteria (Figure 1B, E, C, and D, respectively) are well-known *c*-type tetraheme cytochromes. STC has been implicated in processes that couple the reduction of metal oxides to the oxidation of organic carbon.[5] Cytochrome c_{554} is involved in a biological nitrification pathway.[6] Their hemes have chain-like architectures[6–8] in contrast to those of cyt c_3, the significance of which is the subject of discussion.

For investigation of *c*-type multiheme cytochromes, overproduction has been the major problem. Conventional *Escherichia coli* expression systems do not work.[9] The most popular host cell for the expression is *D. desulfuricans* G200.[10] However, it suffers from poor yields. We have established an overexpression system for *c*-type multiheme cytochromes, using *Shewanella oneidensis* (*So*) cells and *E. coli* plasmids,[11] which was used in the following work. An *E. coli* expression system involving coexpression of *c*-type cytochrome maturation genes has also been reported.[12]

Factors Regulating the Extremely Low Reduction Potentials of Cytochrome c_3

The major factors regulating the reduction potential of a heme iron in a heme protein have been indicated to be the nature of the coordination bonds, and the polarity and charges around the heme.[13] The reduction potentials of cyt c_3 are lower than those of mitochondrial cyt *c* by about 500 mV despite their similar pI values (around 10); there are similar contributions from charges. The most significant difference is found in the sixth ligand, which is
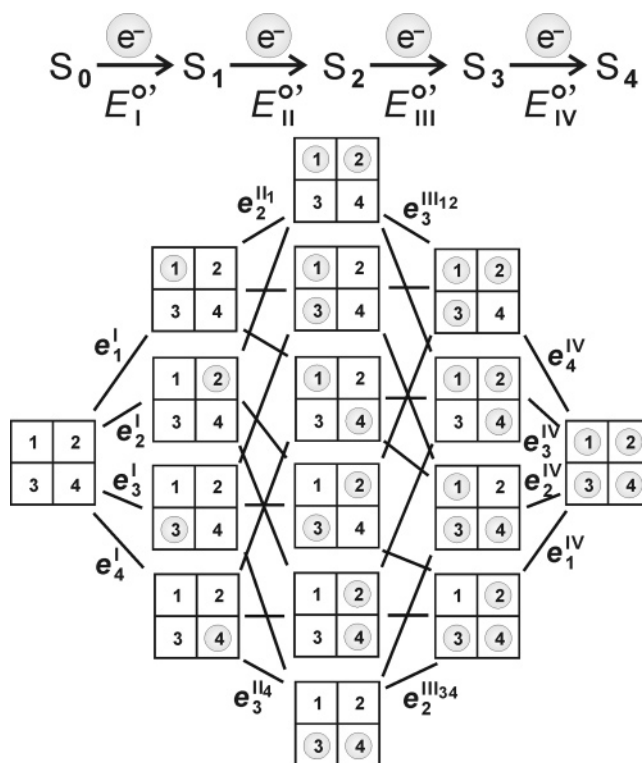
FIGURE 2. Five macroscopic oxidation states, and macroscopic and microscopic reduction potentials. Macroscopic reduction potentials, $E_i^{o\prime}$, are for between two states, S_{i-1} and S_i ($i = 1-4$). The microscopic reduction potential of heme *j* at the *k*th reduction step with heme *m* already reduced is represented by e_j^{km}. Figures in boxes stand for heme numbering.

Table 1. Macroscopic Reduction Potentials of Cytochromes c_3 Isolated from Various Species

strain	$E_I^{o\prime}$	$E_{II}^{o\prime}$	$E_{III}^{o\prime}$	$E_{IV}^{o\prime}$/mV	ref
Desulfovibrio vulgaris Miyazaki F	−242	−296	−313	−358	3
D. vulgaris Hildenborough	−280	−320	−350	−380	35
D. desulfuricans ATCC27774	−140	−260	−370	−380	36
D. gigas	−205	−280	−285	−340	37
D. africanus (basic form)	−90	−260	−280	−290	38
D. africanus (acidic form)	−210	−240	−260	−270	38
Desulfomicrobium norvegicum	−220	−280	−310	−350	38

histidine (His) for cyt c_3 in contrast to methionine (Met) for cyt *c*. The replacement of axial His by Met results in an increase in the macroscopic reduction potential by 40– 185 mV on average.[14] Furthermore, the heme exposure is much greater for cyt c_3 than for cyt *c*.[15] This increases the polarity around the hemes of cyt c_3 and lowers its reduction potentials. However, these factors are not enough to explain the lowering mechanism in view of the reduction potentials of *So* STC, which are −192 mV on average at pH 7 in comparison with −302 mV for *Dv*MF cyt c_3. Their pIs are 5.8 and 10.5, and their average heme exposures are 229 and 144 Å^2, respectively. Because negative charges and higher polarity stabilize an oxidized heme, the reduction potentials of STC should be lower than those of cyt c_3, which is not the case. Therefore, unknown factors around hemes and/or the cyclic heme architecture in cyt c_3 should also be responsible for its extremely low reduction potentials.[16]
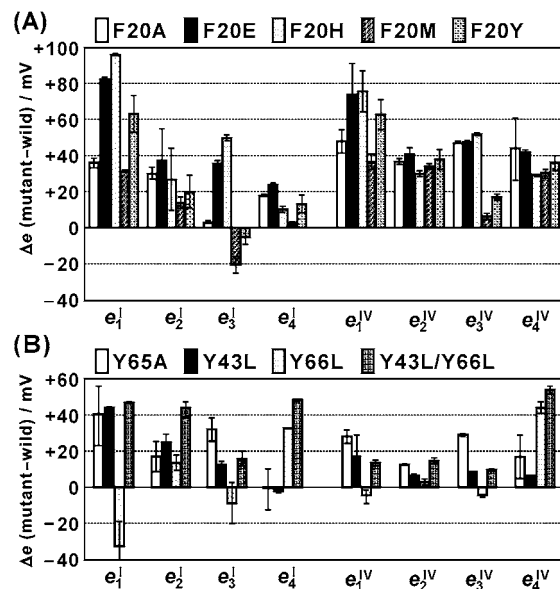
Table 2. Microscopic Reduction Potentials at the First and Fourth Reduction Steps ($e_i{}^I$ and $e_j{}^{IV}$, Respectively),[a] and Interacting Potentials between Hemes *m* and *n* (I_{mn}) of Cytochrome c_3 Isolated from *Desulfovibrio vulgaris* Miyazaki F at pH 7

Microscopic Reduction Potentials at First and Fourth Reduction Steps/mV							
$e_1{}^I$	$e_2{}^I$	$e_3{}^I$	$e_4{}^I$	$e_1{}^{IV}$	$e_2{}^{IV}$	$e_3{}^{IV}$	$e_4{}^{IV}$
−308	−325	−286	−252	−293	−315	−344	−308

Interacting Potentials/mV					
I_{12}	I_{13}	I_{14}	I_{23}	I_{24}	I_{34}
+30	−13	−2	−6	−15	−39

[a] Subscripts denote heme numbers.
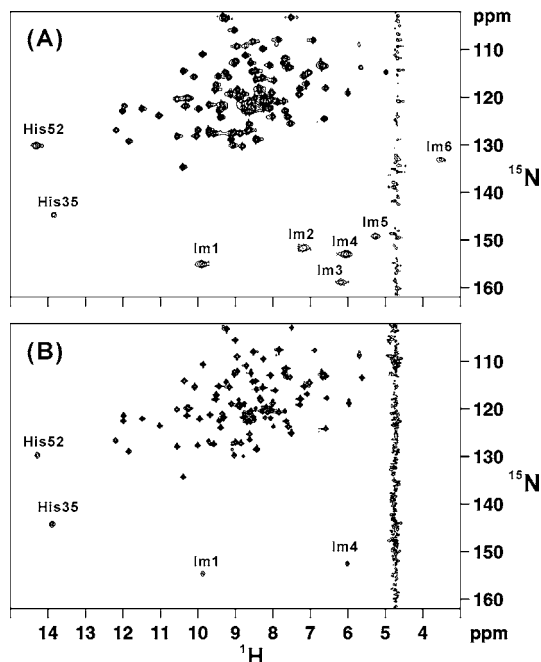
FIGURE 3. ^1H–^{15}N HMQC spectra of uniformly ^{15}N-labeled ferric cytochrome c_3 at (A) pH 5 and (B) pH 7. Imidazole imide signals are indicated by either the residue number or the Im. The assignment will be given elsewhere.

FIGURE 4. Differences in the microscopic reduction potentials between the wild-type and mutant cytochromes c_3.[19] Mutations (A) at Phe20, and (B) at Tyr43, Tyr65, and Tyr66. The types of mutations are indicated at the top. Error bars are given in the figure. Reproduced with permission from ref 19. Copyright 2004 American Chemical Society.

Electron paramagnetic resonance (EPR) analysis of a single crystal of oxidized cyt c_3 suggested that the axial ligands of hemes 1, 3, and 4 have an imidazolate-like nature, those of heme 4 being the strongest.[17] Actually, the ^1H–^{15}N HMQC (heteronuclear multiple-quantum coherence) NMR spectrum of cyt c_3 contained eight signals of coordinated imdazole imides at pH 5, but four of those signals disappeared at pH 7 (Figure 3, unpublished data). Noncoordinated His67 does not give a signal because of its low pK_a. Because two signals of heme 2 (His35 and His52) could always be seen, the disappearing signals can be ascribed to hemes 1, 3, and/or 4, the imidazoles of which should have lower pK_a values than usual. This is in good agreement with the implications from EPR analysis. In the crystal structure, however, it is difficult to identify corresponding differences explicitly, although all coordinated imidazoles are involved in hydrogen bonding with surrounding residues.[15,18] The imidazolate-like nature of the ligands stabilizes the oxidized form of the relevant heme, resulting in a decrease in its reduction potential.

Aromatic rings have been suggested to be involved in electron transfer and redox regulation.[15] Because there are many aromatic residues in cyt c_3, systematic analysis of these residues was performed.[18,19] The aromatic residues in *Dv*MF cyt c_3 can be classified into three groups. The aromatic rings of Phe20, Tyr43, Tyr66, and Phe76 are parallel to the imidazole rings of coordinated histidines at hemes 3, 1, 4, and 2, respectively. On the other hand, the side chains of Tyr65 and His67 form hydrogen bonds with the propionate carboxyl groups of hemes 4 and 2, respectively. The third group comprises heme ligands. Their roles were elucidated by site-directed mutagenesis at every aromatic residue except for axial ligands.

The effects of mutations on the microscopic reduction potentials are summarized in Figure 4, except those at His67 and Phe76, which exhibited little effect. The effect was greatest for Phe20 in contrast to earlier results.[20,21] This is consistent with the highest conservation of this residue in the sequence of cyt c_3. Although the aromatic ring of Phe20 is parallel to the porphyrin ring of heme 1 and the imidazole ring of the sixth ligand of heme 3, the effect of the mutation was more significant for heme 1. Furthermore, the effect on heme 1 was the greatest (an increase of 60−90 mV) for the replacements by polar amino acids (F20E, F20H, and F20Y). Thus, it can be

concluded that the hydrophobicity is more important than the aromaticity for heme 1. In contrast, the reduction potentials of heme 3 were hardly affected by mutation F20Y, suggesting that the aromaticity is important for heme 3. Mutations at Tyr43 and Tyr66 revealed the importance of aromaticity and its local nature. The loss of the $\pi-\pi$ interaction between the aromatic ring of Tyr and the axial imidazole caused increases in the reduction potentials of local hemes by 30−50 mV. The hydrogen bonding with a propionate showed little effect. The aromatic residues shown in Figure 4 are conserved in the cyt c_3 subfamily with CXXC, CXXXXC, CXXC, and CXXXXC heme attachment motifs (C and X represent cysteine and any amino acid, respectively).[19] On the other hand, elimination of the hydrogen bond between Thr24 and His25 was reported to increase the reduction potential of heme 3 in *Dv*H cyt c_3 by about 100 mV.[22] We have confirmed this for *Dv*MF cyt c_3, although the change was not so large (unpublished data). This effect is also local.

Although there is no factor beside the bis-imidazole coordination and large solvent-exposure for heme 2, its redox potential is as low as those of other hemes. Interheme interactions in the cyclic heme architecture seem to play a role in maintaining the low reduction potentials of all hemes. Because an electron is hopping around all hemes, the whole system acts as a single redox center, which would average the major reduction potentials of four hemes to a certain extent. In addition to this, the local contributions mentioned above would make the potentials of individual hemes different.

Roles of Individual Hemes in the Cyclic Heme Architecture in Electron Transport

The functional roles of individual hemes were investigated in the interaction of *Dv*MF cyt c_3 with the physiological partner of cyt c_3, [NiFe] hydrogenase.[23] Hydrogenase catalyzes the reversible oxidoreduction between molecular hydrogen and proton ions, cyt c_3, thereby acting as an electron acceptor or donor. This is one of the core reactions in the hydrogen cycling for energy production in the genus *Desulfovibrio*.[1] The [NiFe] hydrogenase from *Dv*MF is a heterodimeric protein. Its small subunit ($M_r \approx$ 29 000) contains three iron sulfur clusters, proximal [4Fe4S], medial [3Fe4S], and distal [4Fe4S], which are allocated linearly from the active center to the molecular surface (Figure 6). The Ni−Fe active center, on the other hand, is located in the large subunit ($M_r \approx$ 63 000).[24] Although the interaction between cyt c_3 and hydrogenase has been studied for some systems,[23] there has been no structural investigation on pairs from the same bacterial species. The sole related report was on NMR measurements and structural modeling for [Fe] hydrogenase from *D. desulfuricans* and cyt c_3 from *Dv*H.[25]

We have investigated a homologous system, *Dv*MF cyt c_3 and *Dv*MF [NiFe] hydrogenase, to elucidate the mechanism of electron transport between them.[23] The chemical shifts of ^{1}H−^{15}N HSQC cross-peaks of uniformly ^{15}N-labeled ferric cyt c_3 were measured in the absence and
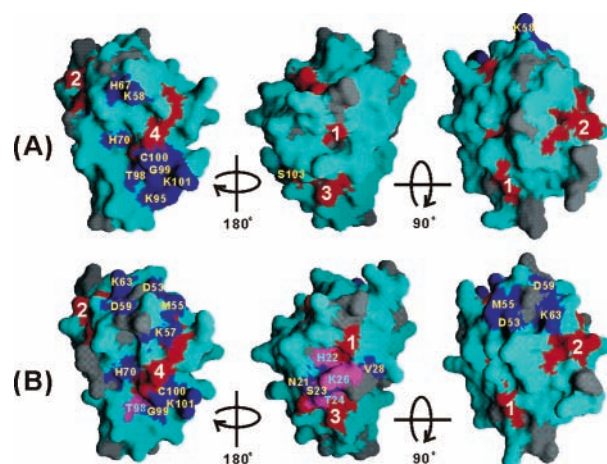

FIGURE 5. Chemical shift perturbation mapping of (A) ferric and (B) ferrous cytochrome c_3 on the crystal structure and solution structure, respectively (PDB entries 1J0O and 1IT1).[23] Residues are colored according to the following classification. Dark blue, $\Delta\delta_{ave}$ $\geq$ 0.02 (A) or 0.05 (B) ppm; gray, unassigned; magenta, not detected; and red, hemes. Sequential and heme numbers are given. Reproduced with permission from ref 23. Copyright 2006 American Chemical Society.

presence of the fully oxidized [NiFe] hydrogenase, respectively. The same measurement was carried out for ferrous ^{15}N-cyt c_3 and the fully reduced hydrogenase. The residues showing large chemical shift perturbations were mapped on the ferric and ferrous cyts c_3 structures, respectively (Figure 5). For the ferric type, chemical shift changes were observed only around heme 4. For the ferrous type, however, the residues between hemes 1 and 3 were affected in addition to those around heme 4. At the first reduction step, the reduction potential of heme 4 is the highest at pH 7 (Table 2). Therefore, heme 4 is the most suitable electron acceptor from a thermodynamic point of view. This supports the idea that heme 4 is the physiological interaction site in the electron transport from hydrogenase to cyt c_3.

The mode of interaction between cyt c_3 and [NiFe] hydrogenase in the oxidized state was investigated in detail by modeling the transient complex,[23] using docking-software ZDOCK.[26] On the basis of the structural architectures of metal centers, the distal [4Fe4S] cluster of hydrogenase was suggested to interact with the redox center of a counterpart.[24] Thus, the subset of complexes with heme 4 close to the distal [4Fe4S] cluster were selected from those predicted. The two structures with the lowest energies are shown in Figure 6. The distance between the edges of heme 4 and the distal [4Fe4S] cluster is 6.5 and 6.4 Å for model nos. 1 and 2, respectively. To determine the role of surface residues in electron transport, 10 lysine residues, mainly around heme 4, were substituted by Met, respectively. The effects of the lysine mutations on the reduction potentials were small (less than 10 mV).[23] In contrast, the mutations affected the kinetics of reduction of cyt c_3 by hydrogenase to varying extents. Both structures in Figure 6 are consistent with the effects of the mutations on the cyt c_3 reduction kinetics. The residues showing the greatest effects (Lys60,
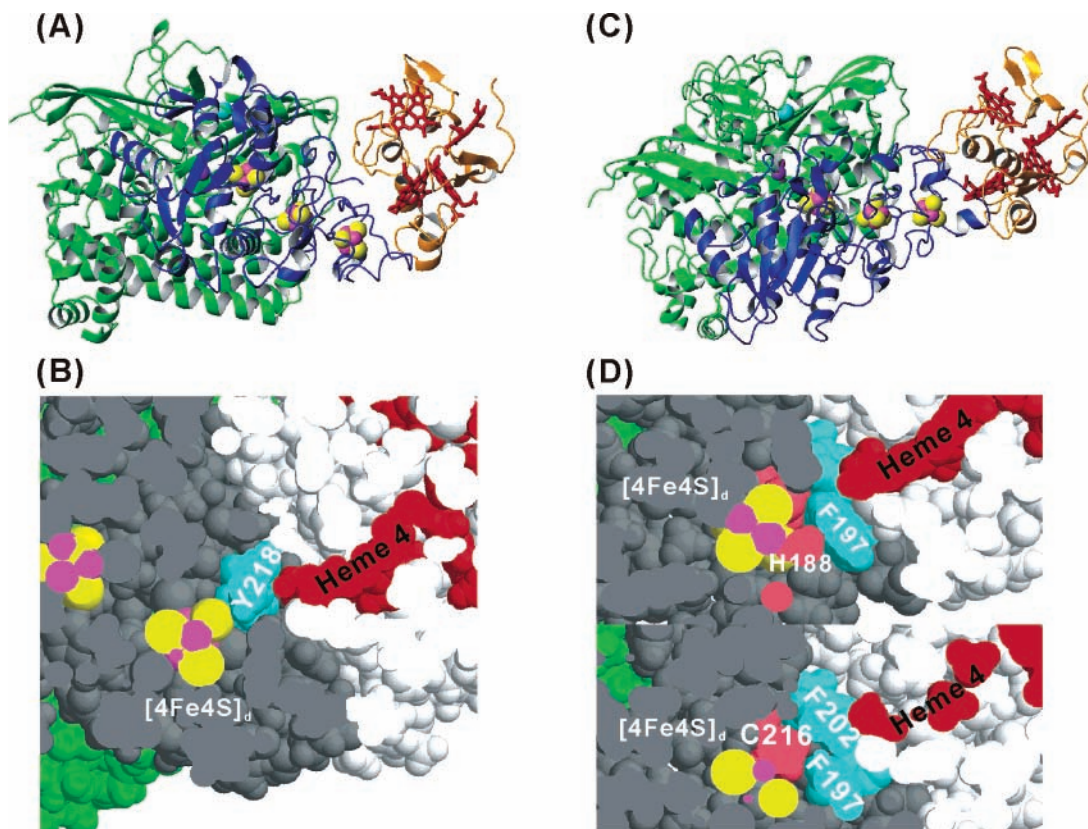
FIGURE 6. The model structures of the ferric cytochrome c_3-[NiFe] hydrogenase complexes.[23] (A and C) Overall structures of model nos. 1 and 2, respectively. Cytochrome c_3, and the large and small subunits of hydrogenase, are colored orange, green, and blue, respectively. (B and D) Interface regions of model nos. 1 and 2, respectively. Heme, iron, sulfur, and nickel are colored red, magenta, yellow, and purple, respectively. Aromatic residues and ligands of the distal [4Fe4S] cluster are colored cyan and pink, respectively. Reproduced with permission from ref 23. Copyright 2006 American Chemical Society.

Lys72, Lys95, and Lys101) are included in the sites of interaction between the two proteins on complex formation. In model no. 1, [4Fe4S]$_d$−Tyr218−heme 4 is the putative electron-transfer pathway (Figure 6B). In model no. 2, two pathways ([4Fe4S]$_d$−His188−Phe197−heme 4 and [4Fe4S]$_d$−Cys216−Phe202−heme 4) are possible (Figure 6D). His188 is the ligand of the distal [4Fe4S] cluster and unique to [NiFe] hydrogenase, and the aromatic ring of Phe197 is perfectly conserved as either Phe or Tyr in the [NiFe] hydrogenase gene, *hynS*. Therefore, the chain of the distal [4Fe4S] cluster−His188−aromatic ring (Phe197) seems to be a conserved pathway for the electron delivery from hydrogenase.

The results mentioned above clearly revealed that heme 4 acts as the electron acceptor in the reduction by [NiFe] hydrogenase, as suggested by earlier work.[23] An important finding for the reduced state is the appearance of a new perturbed site around heme 3. The chemical shift perturbation at Cys79, which links heme 3, was one of the largest. The resonances of Asn21−Lys26 and Val28, which are situated between hemes 3 and 1, either disappeared or shifted significantly. These perturbations might indicate either a new interaction site for hydrogenase or secondary effects of binding to other sites. If the latter is the case, the binding site should be heme 4. Because the region around heme 3 was not affected in the oxidized state, this kind of secondary effect is unlikely. Therefore, the region

around heme 3 is a candidate for the interaction site for the electron transport from cyt c_3 to hydrogenase. Actually, heme 3 is the most suitable electron donor with the lowest potential in the fully reduced state (Table 2). Therefore, even if hemes 3 and 4 were involved in the interaction, heme 3 would act as a more efficient gate for the electron delivery to hydrogenase. This indicates that individual hemes may play different roles in the electron donation and acceptance.

A Regulatory Unit in the Cyclic Heme Architecture

Carbon monoxide (CO) has been reported to bind to cyt c_3.[27] CO is well known to strongly bind to five-coordinated ferrous heme in a protein, inhibiting its biological function. However, cyt c_3 carries only six-coordinated hemes. Thus, the nature of CO binding to cyt c_3 is intriguing. The visible absorption spectrum of fully reduced cyt c_3 on CO titration is presented in Figure 7A.[27] It is clear that all four hemes can bind CO because ferrous heme bands at 552 and 523 nm are lost at high CO concentrations. Taking this into account, the formation of CO-bound heme was plotted as a function of CO concentration in Figure 7B. The first CO binding gave a typical saturation curve, although the curve becomes complicated at higher CO concentrations. The K_d for single CO binding was 8.0 $\pm$
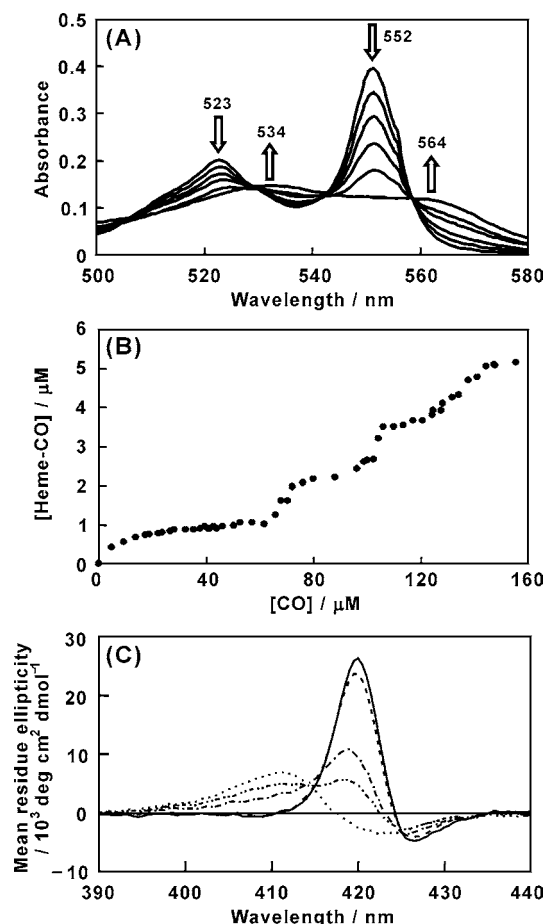
FIGURE 7. CO titration of fully reduced cytochrome c_3 at pH 7.0 and 25 °C.[27] (A) Visible absorption spectra in the presence of 0, 28, 75, 113, 142, and 377 μM CO. (B) The amount of CO-bound heme as a function of CO concentration. (C) Circular dichroism spectra in the presence of 0.0, 40.9, 81.8, 122.7, and 188.7 μM CO (from solid to dotted lines, respectively). The concentration of cyt c_3 was 3.3 μM for (A), 1.3 μM for (B), and 4 μM for (C).

0.2 μM. To examine the effect of CO binding on the cyt c_3 structure, circular dichroism (CD) spectra were obtained. The results revealed that, while the CD spectrum of the single-CO bound cyt c_3 (CO-cyt c_3) remained almost intact, binding of more CO molecules induced a significant change in CD, suggesting a structural alteration including the heme architecture (Figure 7C). In contrast to CO, O_2 only oxidizes the reduced cyt c_3 without binding. NO also did not bind to it. Therefore, cyt c_3 specifically binds CO, which means that it is a potential CO sensor. The first CO was found to bind to the sixth coordination site of heme 2 on NMR.[27] The specific replacement of His35 by CO indicates that the original coordination bond is weak. In fact, the $N_{\epsilon 2}$–Fe bond of His35 is among the longest in this protein.[15,18] Heme 2 is also unique in view of the structure of triheme cytochrome c_7 (cyt c_7). Cyt c_7 has a heme architecture similar to that in cyt c_3, but lacks heme 2.[28] Therefore, the architecture of active hemes in CO-cyt c_3 is similar to that in cyt c_7, which is physiologically active *in vivo*.

Surprisingly, *D. vulgaris* can grow on CO, using it as a sole electron donor.[29] The activity of [NiFe] hydrogenase, however, is known to be inhibited by CO. Because CO-cyt c_3 cannot receive electrons from [NiFe] hydrogenase, it must receive them from other proteins. Actually, *D. vulgaris* carries the CO-related *coo* genes, which include CO-dehydrogenase and CO-induced hydrogenase (Gen-Bank accession number NC_002937). The latter is expected to be CO-resistant. Furthermore, in the absence of conventional hydrogenase, CO accumulation takes place.[30] In its first stage, an electron transport system for sulfate reduction is still working without conventional hydrogenase and in the presence of CO. CO-cyt c_3 may be involved in this electron transport, because the maximum level of physiological CO accumulation was about 7.6 μM for *D. vulgaris* and the K_d for single CO-binding to cyt c_3 is 8.0 μM. If this is the case, cyt c_3 acts as a security device on accumulation of potentially toxic CO. CO becomes actually toxic for sulfate-reducing bacteria at more than 42 μM,[29] which would induce the inactivation of cyt c_3 through a structural change on the second CO binding (Figure 7B and C).

CO-sensor proteins reported so far have one regulatory and one functional domain. Although cyt c_3 apparently has just one domain, the tetraheme architecture can be taken as a multi-unit structure with heme 2 being the regulatory unit. Heme 2 would play a regulatory role in switching electron transport pathways on the occasion of an environmental change induced by CO. The cyclic heme architecture makes this kind of regulation efficient.

Biological Significance of Heme Architectures

In contrast to that of cyt c_3, a chain-like heme architecture is expect to act in a different manner. STC from *So* contains 91 amino acid residues and four *c*-type hemes arranged in a chain-like form (Figure 1B). Both the fifth and the sixth axial ligands are imidazoles of His for all hemes, just as for cyt c_3.[7] The macroscopic and microscopic reduction potentials of the four hemes of *So* STC have been determined.[16] The latter at pH 7.0 is shown for each heme in Figure 8. The ordinate corresponds to the free energy. The reduction fractions on the top revealed that the order of reduction is from hemes in the C-terminal domain (hemes 3 and 4) to that in the N-terminal domain (heme 1), demonstrating the polarization of the tetraheme chain during reduction. This is in a sharp contrast to the reduction profiles of cyt c_3 (Figure 8). Taking the low solvent exposure of heme 3 into account, heme 4 is the most efficient electron delivery site. Thus, this architecture provides a pathway for directional electron transfer.

Furthermore, this heme architecture can be used for multi-electron reduction of a redox partner through heme 4. The reduction potential of heme 4 in each reduction step always becomes lowest (highest in energy) when an electron stays at heme 3 (e_4^{II3} and e_4^{III3} in Figure 8). It provides more driving force for reduction of the redox partner by electron delivery through heme 4. Moreover, because heme 3 is reduced, the electron would move to the oxidized heme 4 immediately after the electron
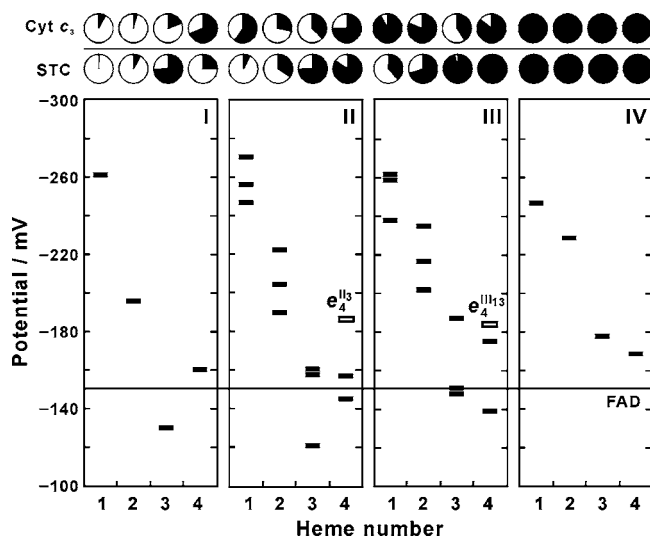
FIGURE 8. Microscopic reduction potentials and reduction fractions of four hemes of *Shewanella oneidensis* STC at pH 7.0 with 300 mM KCl. Microscopic reduction potentials are indicated by bars for each heme. I, II, III, and IV stand for the reduction steps. Because there are e_4^{III13}, e_4^{III12}, and e_4^{III23} for heme 4 at the third reduction step, for example, three bars are drawn for each heme in panels II and III. The reduction fraction of each heme after the relevant reduction step is presented at the top as a dark area in a circle for STC (lower) and cytochrome c_3 (upper). The reduction potential of flavin adenine dinucleotide (FAD) in *S. frigidimarina* flavocytochrome *c* is given by a solid line.[39]

delivery, thus facilitating cooperative two-electron reduction through concerted electron transfer. This mechanism likely participates in the two-electron reduction of the flavin in SFR (also called flavocytochrome *c*). The cytochrome domain of *So* SFR exhibits 34% identity with *So* STC.[31] The crystal structure of *So* SFR[32] revealed that the architecture of the cytochrome domain of SFR is almost identical to that of STC (Figure 1B and E). Also, heme 4 is the site that makes contact with the target redox center, flavin. The flavin in SFR converts fumarate to succinate through two-electron reduction. The reduction potential of the flavin is indicated in Figure 8. Once electrons get to heme 1, they will move all of the way to heme 4 and will be delivered to flavin one after another in a downhill manner when there is a substrate. Here, the heme architecture acts as a molecular wire with a two-electron reduction module in contrast to the cyclic heme architecture in cyt c_3.

RCC also has a chain-like heme architecture (Figure 1D). Three sixth ligands are Met, and the other is His. Their reduction potentials are higher than those of cyt c_3 and STC. They are +380 (heme III), +30 (heme IV), +310 (heme II), and −70 mV (heme I) from the reaction center to the other side for *Blastochloris viridis* (former *Rhodopseudomonas*).[33] The electrostatic effects on the midpoint potentials of four hemes were reported.[13] Heme III supplies an electron to the special pair in the reaction center. The high-potential iron−sulfur protein is one of the electron donors to RCC.[34] It is assumed to interact with heme I and to deliver an electron in an uphill manner, and then the electron moves to heme III.[34] Thus, this

chain-like architecture also acts as a molecular wire, although the role of the high-potential heme II is not yet clear. Now, we can conclude that the heme architectures in tetraheme cytochromes are carefully designed for their biological functions.

Concluding Remarks

The investigations mentioned above clearly revealed that the tetraheme cytochromes *c* are not simple heme assemblies but sophisticated devices. In the cyclic heme architecture, each heme behaves like a domain in multidomain proteins. Each domain has specific functions, including a regulatory one. This would be an efficient way to organize redox reactions necessary for living processes of primitive organisms. It can also save polypeptides and corresponding genes, which would need more energy to maintain. In contrast, the chain-like architecture functions as a regulated molecular wire. Although the regulatory mechanisms have not yet been fully clarified, the two-electron reduction module is one of them.

References

(1) Odom, J. M., Singleton, R., Jr., Eds. *The Sulfate-Reducing Bacteria: Contemporary Perspectives*; Springer-Verlag: New York, 1993.

(2) Harada, E.; Fukuoka, Y.; Ohmura, T.; Fukunishi, A.; Kawai, G.; Fujiwara, T.; Akutsu, H. Redox-coupled conformational alterations in cytochrome c_3 from *D. vulgaris* Miyazaki F on the basis of its reduced solution structure. *J. Mol. Biol.* **2002**, *319*, 767−778.

(3) Park, J.-S.; Ohmura, T.; Kano, K.; Sagara, T.; Niki, K.; Kyogoku, Y.; Akutsu, H. Regulation of the redox order of four hemes by pH in cytochrome c_3 from *D. vulgaris* Miyazaki F. *Biochim. Biophys. Acta* **1996**, *1293*, 45−54.

(4) Louro, R. O. Proton thrusters: overview of the structural and functional features of soluble tetrahaem cytochrome c_3. *J. Biol. Inorg. Chem.* **2007**, *12*, 1−10.

(5) Myers, C. R.; Myers, J. M. Outer membrane cytochromes of *Shewanella putrefaciens* MR-1: spectral analysis, and purification of the 83-kDa *c*-type cytochrome. *Biochim. Biophys. Acta* **1997**, *1326*, 307−318.

(6) Iverson, T. M.; Arciero, D. M.; Hsu, B. T.; Logan, M. S.; Hooper, A. B.; Rees, D. C. Heme packing motifs revealed by the crystal structure of the tetra-heme cytochrome c_{554} from *Nitrosomonas europaea*. *Nat. Struct. Biol.* **1998**, *5*, 1005−1012.

(7) Leys, D.; Meyer, T. E.; Tsapin, A. S.; Nealson, K. H.; Cusanovich, M. A.; Van Beeumen, J. J. Crystal structures at atomic resolution reveal the novel concept of "electron-harvesting" as a role for the small tetraheme cytochrome *c*. *J. Biol. Chem.* **2002**, *277*, 35703−35711.

(8) Deisenhofer, J.; Epp, O.; Sinning, I.; Michel, H. Crystallographic refinement at 2.3 Å resolution and refined model of the photosynthetic reaction centre from *Rhodopseudomonas viridis*. *J. Mol. Biol.* **1995**, *246*, 429−457.

(9) Pollock, W. B.; Chemerika, P. J.; Forrest, M. E.; Beatty, J. T.; Voordouw, G. Expression of the gene encoding cytochrome c_3 from *Desulfovibrio vulgaris* Hildenborough in *Escherichia coli*: export and processing of the apoprotein. *J. Gen. Microbiol.* **1989**, *135*, 2319−2328.

(10) Voordouw, G.; Pollock, B.; Bruschi, M.; Guerlesquin, F.; Rapp-Giles, B.; Wall, J. D. Functional expression of *Desulfovibrio vulgaris* Hildenborough cytochrome c_3 in *Desulfovibrio desulfuricans* G200 after conjugational gene transfer from *Escherichia coli*. *J. Bacteriol.* **1990**, *172*, 6122−6126.

(11) Ozawa, K.; Yasukawa, F.; Fujiwara, Y.; Akutsu, H. A simple, rapid, and highly efficient gene expression system for multiheme cytochrome *c*. *Biosci. Biotechnol. Biochem.* **2001**, *65*, 185−189.

(12) Arslan, E.; Schulz, H.; Zufferey, R.; Künzler, P.; Thöny-Meyer, L. Overproduction of the *Bradyhizobium japonicum c*-type cytochrome subunits of the *ccb₃* oxidase in *Escherichia coli*. *Biochem. Biophys. Res. Commun.* **1998**, *251*, 744–747.

(13) Gunner, M. R.; Honig, B. Electrostatic control of midpoint potentials in the cytochrome subunit of the *Rhodopseudomonas viridis* reaction center. *Proc. Natl. Acad. Sci. U.S.A.* **1991**, *88*, 9151–9155.

(14) Dolla, A.; Florence, L.; Bianco, P.; Haladjian, J.; Voordouw, G.; Forest, E.; Wall, J.; Guelresquin, F.; Bruschi, M. Characterization and oxidoreduction properties of cytochrome *c₃* after heme axial ligand replacements. *J. Biol. Chem.* **1994**, *269*, 6340–6346.

(15) Higuchi, Y.; Kusunoki, M.; Matsuura, Y.; Yasuoka, N.; Kakudo, M. Refined structure of cytochrome *c₃* at 1.8 Å resolution. *J. Mol. Biol.* **1984**, *172*, 109–139.

(16) Harada, E.; Kumagai, J.; Ozawa, K.; Imabayashi, S.; Tsapin, A. S.; Nealson, K. H.; Meyer, T. E.; Cusanovich, M. A.; Akutsu, H. A directional electron transfer regulator based on heme-chain architecture in the small tetraheme cytochrome *c* from *Shewanella oneidensis*. *FEBS Lett.* **2002**, *532*, 333–337.

(17) Saitoh, T.; Tachibana, Y.; Higuchi, Y.; Hori, H.; Akutsu, H. Correlation between the *g* tensors and the nonplanarity of porphyrin rings in *Desulfovibrio vulgaris* Miyazaki F cytochrome *c₃*, studied by single crystal EPR. *Bull. Chem. Soc. Jpn.* **2004**, *77*, 357–363.

(18) Ozawa, K.; Takayama, Y.; Yasukawa, F.; Ohmura, T.; Cusanovich, M. A.; Tomimoto, Y.; Ogata, H.; Higuchi, Y.; Akutsu, H. Role of the aromatic ring of Tyr43 in tetraheme cytochrome *c₃* from *Desulfovibrio vulgaris* Miyazaki F. *Biophys. J.* **2003**, *85*, 3367–3374.

(19) Takayama, Y.; Harada, E.; Kobayashi, R.; Ozawa, K.; Akutsu, H. Roles of noncoordinated aromatic residues in redox regulation of cytochrome *c₃* from *Desulfovibrio vulgaris* Miyazaki F. *Biochemistry* **2004**, *43*, 10859–10866.

(20) Saraiva, L. M.; Salgueiro, C. A.; LeGall, J.; van Dongen, W. M. A. M.; Xavier, A. V. Site-directed mutagenesis of a phenylalanine residue strictly conserved in cytochrome *c₃*. *J. Biol. Inorg. Chem.* **1996**, *1*, 542–550.

(21) Dolla, A.; Arnoux, P.; Protasevich, I.; Lobachov, V.; Bruhna, M.; Giudici-Orticoni, M. T.; Haser, R.; Czjzek, M.; Makarov, A.; Bruschi, M. Key role of phenylalanine 20 in cytochrome *c₃*: Structure, stability, and function studies. *Biochemistry* **1999**, *38*, 33–41.

(22) Salgueiro, C. A.; da Costa, P. N.; Turner, D. L.; Messias, A. C.; van Dongen, W. M. A. M.; Saraiva, L. M.; Xavier, A. V. Effect of hydrogen-bond networks in controlling reduction potentials in *Desulfovibrio vulgaris* (Hildenborough) cytochrome *c₃* probed by site-specific mutagenesis. *Biochemistry* **2001**, *40*, 9709–9716.

(23) Yahata, N.; Saitoh, T.; Takayama, Y.; Ozawa, K.; Ogata, H.; Higuchi, Y.; Akutsu, H. Redox interaction of cytochrome *c₃* with [NiFe] hydrogenase from *Desulfovibrio vulgaris* Miyazaki F. *Biochemistry* **2006**, *45*, 1653–1662.

(24) Higuchi, Y.; Yagi, T.; Yasuoka, N. Unusual ligand structure in Ni-Fe active center and an additional Mg site in hydrogenase revealed by high resolution X-ray structure analysis. *Structure* **1997**, *5*, 1671–1680.

(25) ElAntak, L.; Morelli, X.; Bornet, O.; Hatchikian, C.; Czjzek, M.; Doll, A.; Guerlesquin, F. The cytochrome *c₃*-[Fe]-hydrogenase electron-transfer complex: structural model by NMR restrained docking. *FEBS Lett.* **2003**, *548*, 1–4.

(26) Chen, R.; Weng, Z. A novel shape complementarity scoring function for protein–protein docking. *Proteins* **2003**, *51*, 397–408.

(27) Takayama, Y.; Kobayashi, Y.; Yahata, N.; Saitoh, T.; Hori, H.; Ikegami, T.; Akutsu, H. Specific binding of CO to tetraheme cytochrome *c₃*. *Biochemistry* **2006**, *45*, 3163–3169.

(28) Czjzek, M.; Arnoux, P.; Haser, R.; Shepard, W. Structure of cytochrome *c₇* from *Desulfuromonas acetoxidans* at 1.9 Å resolution. *Acta Crystallogr.* **2001**, *D57*, 670–678.

(29) Lupton, F. S.; Conrad, R.; Zeikus, J. G. Physiological function of hydrogen metabolism during growth of sulfidogenic bacteria on organic substrates. *FEMS Microbiol. Lett.* **1984**, *23*, 263–268.

(30) Voordouw, G. Carbon monoxide cycling by *Desulfovibrio vulgaris* Hildenborough. *J. Bacteriol.* **2002**, *184*, 5903–5911.

(31) Tsapin, A. I.; Vandenberghe, I.; Nealson, K. H.; Scott, J. H.; Meyer, T. E.; Cusanovich, M. A.; Harada, E.; Kaizu, T.; Akutsu, H.; Leys, D.; Van Beeumen, J. J. Identification of a small tetraheme cytochrome *c* and a flavocytochrome *c* as two of the principal soluble cytochromes *c* in *Shewanella oneidensis* strain MR1. *Appl. Environ. Microbiol.* **2001**, *67*, 3236–3244.

(32) Leys, D.; Tsapin, A. I.; Nealson, K. H.; Meyer, T. E.; Cusanovich, M. A.; Van Beeumen, J. J. Structure and mechanism of the flavocytochrome *c* fumarate reductase of *Shewanella putrefaciens* MR-1. *Nat. Struct. Biol.* **1999**, *6*, 1113–1117.

(33) Alric, J.; Lavergne, J.; Rappaport, F.; Verméglio, A.; Matsuura, K.; Shimada, K.; Nagashima, K. V. P. Kinetic performance and energy profile in a roller coaster electron transfer chain: A study of modified tetraheme-reaction center constructs. *J. Am. Chem. Soc.* **2006**, *128*, 4136–4145.

(34) Nogi, T.; Hirano, Y.; Miki, K. Structural and functional studies on the tetraheme cytochrome subunit and its electron donor proteins: the possible docking mechanisms during electron transfer reaction. *Photosynth. Res.* **2005**, *85*, 87–99.

(35) Turner, D. L.; Salgueiro, C. A.; Catarino, T.; LeGall, J.; Xavier, A. V. Homotropic and heterotropic cooperativity in the tetrahaem cytochrome *c₃* from *Desulfovibrio vulgaris*. *Biochim. Biophys. Acta* **1994**, *1187*, 232–235.

(36) Morais, J.; Palma, N.; Frazão, C.; Caldeira, J.; LeGall, J.; Moura, I.; Moura, J. J. G.; Carrondo, M. A. Structure of the tetraheme cytochrome from *Desulfovibrio desulfuricans* ATCC 27774: X-ray diffraction and electron paramagnetic resonance studies. *Biochemistry* **1995**, *34*, 12830–12841.

(37) Piçarra-Pereira, M. A.; Turner, D. L.; LeGall, J.; Xavier, A. V. Structure studies on *Desulfovibrio gigas* cytochrome *c₃* by two-dimensional ^{1}H-nuclear-magnetic-resonance spectroscopy. *Biochem. J.* **1993**, *294*, 909–915.

(38) Pieulle, L.; Haladjian, J.; Bonicel, J.; Hatchikian, E. C. Biochemical studies of the *c*-type cytochromes of the sulfate reducer *Desulfovibrio africanus*. Characterization of two tetraheme cytochromes *c₃* with different specificity. *Biochim. Biophys. Acta* **1996**, *1273*, 51–61.

(39) Turner, K. L.; Doherty, M. K.; Heering, H. A.; Armstrong, F. A.; Reid, G. A.; Chapman, S. K. Redox properties of flavocytochrome *c₃* from *Shewanella frigidimarina* NCIMB400. *Biochemistry* **1999**, *38*, 3302–3309.